Analysis of Digital Twin Channel Impulse Response Predictions

Cassie Jeng
College of Engineering
University of California, Berkeley
Berkeley, California, United States
cassie.jeng@berkeley.edu

Neal Patwari
Kahlert School of Computing
University of Utah
Salt Lake City, Utah, United States
neal.patwari@utah.edu

***Abstract*—Next-generation wireless networks will rely on digital twins to model and predict behavior in networks. Ray tracing (RT) is proposed for high-accuracy multipath radio channel modeling. We present a comparative analysis between channel impulse response (CIR) measurements collected on an experimental wireless testbed and the equivalent CIR predictions generated with Sionna RT software, including time delay and amplitude gain statistics of individual multipath components and the channel as a whole. While total multipath power gain of the measured and RT CIRs are correlated with $r = 0.85$, their RMS delay spreads are weakly correlated with $r = -0.35$. Multipath arriving within 100 ns before and after the maximum-power path are predicted well, while those beyond that window are not, having implications for development of digital channel twins.**

***Index Terms*—digital twins, channel impulse response, ray tracing, experimental wireless**

I. Introduction

Digital twins are proposed to allow efficient control of future wireless networks through simulation and prediction [1], e.g., optimizing link capacities in the presence of interference [2], ensuring reliable mobility for vehicular communications systems [3], or auto-configuring a dynamic spectrum sharing system [4]. Ray tracing (RT) is a prevalent digital twin technique that relies on ray optics to estimate path loss, angle of arrival, angle of departure, and time delays in a channel to accurately represent the multipath radio channel [5], [6]. This paper addresses the question: How accurate is RT for digital twinning of the multipath radio channel?

We provide a qualitative and quantitative comparison of channel impulse responses (CIRs) produced through both physical radio channel measurements on the Platform for Open Wireless Data-driven Experimental Research (POWDER), a large outdoor software-defined radio testbed [7], and through the Sionna Ray Tracing (Sionna RT) software [8]. We measure channels in the C-band (3.4 GHz) and with a 26 MHz bandwidth for outdoor links with antenna heights near 10 m. We run Sionna RT with publicly available environment data including building and terrain information. We align the POWDER measured CIR and the Sionna RT predicted CIR to ensure that any amplitude and time uncertainties in the measurements do not count against the RT outputs. In this paper, we present and compare the results graphically and by comparing individual multipath and channel statistics.

As a summary of the presented results, we find that late arriving multipath are relatively poorly predicted by the Sionna RT in our dataset. Knowing the gaps in RT results has implications for future development of digital channel twins, our results contribute to a wider literature studying RT-measurement CIR inaccuracies. Similar observations have been reported as being due to RT's inability to model higher-order specular reflections and non-specular reflections of first-order [9], although the comparison is for 5.6 GHz for relatively short-range links. The measurement results in [10] also found a significant disagreement between the measured and RT RMS delay spreads, with RT exhibiting higher delay spreads. However, the custom RT included non-specular reflections.

This material is based upon work supported by the US National Science Foundation under Grants #2417934, #2346555 and #2232464.

II. Methods

This section specifies our conception of the multipath channel, how we measure the CIR, how we use Sionna RT to predict the CIR, and how we compare the two in the experimental testbed environment.

A. Multipath Channels

We start by defining a channel impulse response model as a sum of L arriving multipath impulses. The ith multipath component has phase ϕ_i, amplitude gain a_i, and time delay τ_i. When the radio channel is assumed to be a linear time invariant (LTI) filter, its CIR is given as [11],

$$h(\tau) = \sum_{i=0}^{L-1} a_i e^{j\phi_i} \delta(\tau - \tau_i). \tag{1}$$

In both our ray tracing model and our measurements, the transmitter and receiver are static, justifying the LTI assumption for our purposes.

B. CIR Measurement

For this comparative analysis, we measure the CIR in the network using maximum length pseudo-noise (PN) codes.

1) Transmitter: We transmit a periodic signal $s(t)$ containing a binary phase-shift keying (BPSK)-modulated PN code signal. The N chips of the PN code are produced using a maximal-length linear feedback shift register (LFSR) with a chip period of τ_c. These are used because the autocorrelation of x, $R_x[n]$, is equal to N when $n = 0$, and -1 otherwise [12]. We use the square-root raised cosine (SRRC) to pulse-shape the chips. The PN code is normalized in amplitude such that the l_2 norm of the code, $\|x\|$ is 1. We refer to one cycle of the PN code signal, $s_1(t)$, as equal to $s(t)$ for $t = 0$ to T_{PN}, where $T_{PN} = N\tau_c$ is the PN code signal duration, and zero otherwise.

In our experiments we transmit $s(t)$ with a sample rate of 56 MHz and chip rate of 28 MHz. Further, to avoid producing unnecessary interference to other operating systems by continuously transmitting, we set $s(t)$ to be three repetitions of the PN code signal.

2) Receiver: We measure the CIR using the received signal $r(t)$ and a copy of the known PN code signal $s_1(t)$. The received signal $r(t)$ is a convolution of the transmitted signal and true channel impulse response $h(t)$, i.e.,

$$r(t) = \gamma h(t) * s(t),$$

where γ is a scale factor including TX power, antenna gains, and unknown measurement system losses. At the receiver, we obtain the correlation function $\rho(\tau)$ by correlating the received signal with the local copy of the PN code signal $s_1(t)$.

$$\rho(\tau) = r(t) * s_1(t) = \gamma \sum_{i=0}^{L-1} a_i e^{j\phi_i} R_{PN}(\tau - \tau_i), \qquad (2)$$

where $R_{PN}(\tau)$ is the autocorrelation function of the PN code. This continuous-time function is approximated as a triangular peak centered at $\tau = 0$ with height 1, width $2\tau_c$ (2 times the chip period), and constant value of $-1/N$ otherwise. Compared to the ideal CIR model of (1), our measurement replaces the impulses with $R_{PN}(\tau)$ [13].

C. Measured Environment

We perform measurements on the POWDER testbed, a publicly and remotely-accessible SDR testbed that is deployed across a 4 km^2 area on the campus of the University of Utah in Salt Lake City [7]. Measurements were collected in the late winter and early spring on days with no reported precipitation. We focus on the results from the *dense deployment* radio nodes in this paper, which use the same hardware and deployment specifications of dense urban "lamp post" style base stations. We first confirm that the nodes are time synchronized using WATCH, a distributed time offset estimation tool for checking time synchronization on the network [14]. Then, we transmit a packet as detailed in publicly available code in the Over-The-Air Channel Impulse Response Tutorial [15], at a center frequency of 3415 MHz. Our implementation is build on top of the openly-available Shout measurement framework, which sends and receives signals approximately simultaneously [14], [16]. The framework iteratively transmits the same designated packet of IQ samples from one transmitting node to all other selected experiment nodes, and then repeats using each node as a transmitter for the remaining nodes. All antennas are omnidirectional in the horizontal plane. The dense deployment nodes in this experiment are time division duplexing (TDD) and have a maximum transmit power of 36 dBm [7].

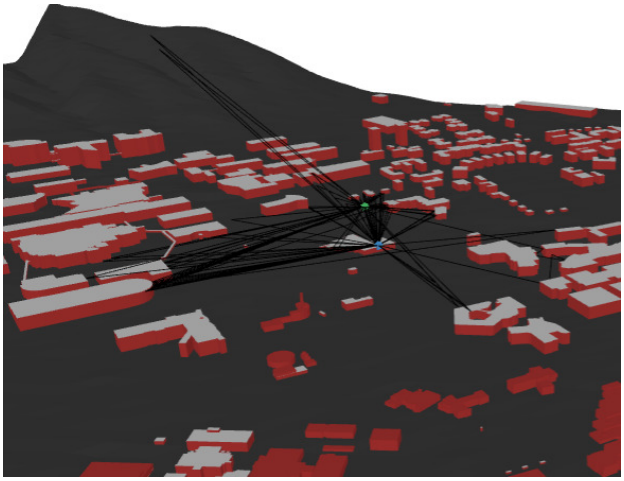

Fig. 1: Rendered ray tracing scene showing transmission path predictions from EBC (•) to Guesthouse (•).

The tutorial calculates $\rho(\tau)$ as described in (2). The output for each receiver reveals the measured CIR. Shout iteratively changes transmitting and receiving nodes, and the end result is a dataset of measured CIRs between all node pairs.

D. Sionna RT

The RT CIR predictions are generated with Sionna RT. This software has become crucial in next-generation wireless research because of its ability to replicate a variety of radio environments, incorporating transmission angles, locations of significant geographic masses, and structural material.

Sionna RT converts a three-dimensional geometric scene for a designated area of interest, drawn from OpenStreetMap, into an XML-file that contains the locations of buildings in the area [8]. For our comparative study, we render a rectangular area encompassing the campus and part of the neighboring mountains, as shown in Fig. 1. Nodes are placed in the scene using their stated latitude-longitude coordinate pairs and antenna heights [17]. We observe that some nodes need manual coordinate and height adjustments to ensure that rooftop nodes are on the roof of the modeled building, and that ground-level dense deployment nodes are not inside of nearby buildings, revealing a first potential cause for mismatch between CIR predictions and measurements. Sionna uses Mitsuba to compute ray intersections with the rendered buildings and TensorFlow to compute reflections with respect to ray tracing parameters like building material, antenna orientations, and antenna positions [8]. The resulting scene shows the predicted transmissions for a specified link, including both LOS paths and any reflections from surrounding buildings and geography.

This ray tracing simulation is carried out with both diffraction and reflection enabled, and the locations of the nodes, allowing a visualization of all predicted paths with an emphasis on arriving multipath signals.

E. CIR Matching

To allow for a direct comparison between the measured and RT CIR amplitudes, we scale the measured CIR amplitude by a factor $1/\hat{\gamma}$, determined to match the ratio of the highest amplitude peaks in both measured and RT data. Because the time axis of the measured CIR can be in error due to unknown time delays on the order of a μs [14], we align the time axes of the two CIRs by shifting the time axis of the measured CIR so that the time of arrival of the highest amplitude peak in the measured CIR matches that of the RT CIR.

F. Peak Comparison Metrics

To further examine how well the Sionna RT prediction aligns with the measured CIRs, we present a method to iterate through the RT predicted multipath and compare their time and magnitude to the surrounding measurements from the experimental CIR data.

As the experimental data includes noise from the channel, we experimentally determine a link-dependent noise floor threshold as

$$n_{thresh} = 3.4\sqrt{2}\ \sigma_n, \tag{3}$$

where σ_n is the standard deviation of a noise array formed by removing the two most prominent peaks in the measured CIR. The scalar in (3) was visually optimized on the measured CIR plots to remove noise before and after the prominent peaks.

The algorithm analyzes each predicted multipath's similarity to surrounding measured peaks. For each peak in the RT prediction, we focus on the measured CIR within $2\tau_c$ (twice peak width) of the RT multipath. We disregard any measured CIR samples below the calculated noise floor threshold and search through the remaining measured samples to determine if there are any peaks that could indicate a multipath arrival. Any potential measured multipath peak is compared in amplitude and arrival time to the RT path. A match is determined if the RT multipath and the measured CIR peak are less than $2\tau_c$ apart, and their amplitudes differ by less than half the magnitude of the lower-amplitude peak. In other words, the power (squared magnitude) difference is less than 3.5 dB. Fig. 2 shows a resulting plot for a well-aligned RT path (●) on the EBC → Guesthouse link with the measured CIR data (—) and detected matching local peak (■). Because our peak comparison method iterates through the RT multipath, some plots show additional RT paths that happen to arrive close in time to other paths. Fig. 2 includes an additional RT path arriving just before 1μs, but this path is determined to not be a match due to its large amplitude difference with the temporally-close peak (■).

While the predicted multipath and measured peak in Fig. 2 are only 23 ns apart and their magnitudes differ by less than half the magnitude of the lower-amplitude peak, allowing them to be classified as a match, we also observe that across all

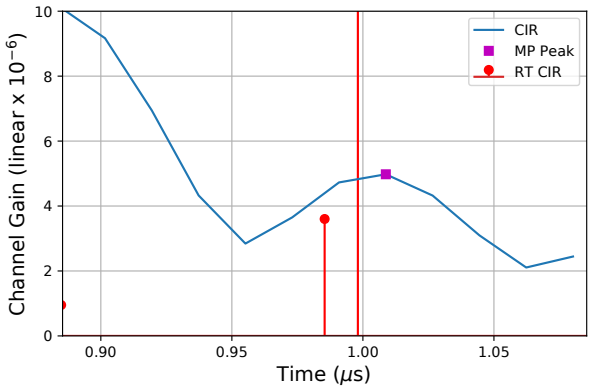

Fig. 2: Algorithm plot for well-aligned RT peak in the EBC → Guesthouse link showing a match found for measured CIR multipath peak (■) and RT CIR path (●).

links, there are many RT predicted multipath that do not align well with measured CIR peaks.

In addition to comparing the amplitude and delays of individual paths, we also compare multipath power gain, root-mean-square (RMS) delay spread, and mean delay.

We use a peak-finding algorithm to isolate the local peaks throughout the measured CIR data. These local peaks are used in further analysis to calculate multipath power gain and RMS delay spread for the measured data. For our experiments, $2\tau_c = 100$ ns, so we analyze the RT multipath detected within 100 ns before and after each measured CIR peak. We also crop both measured and RT CIR data arrays to limit our focus to the peaks found within approximately 1 μs of the prominent peak. This avoids unrealistically large power and delay spread values from using the entire PN code duration T_{PN}, including noise measurements from before the first peak and after the last detectable multipath in the channel.

G. CIR Statistics

We use several summary statistics often used to characterize multipath channels.

a) Multipath Power Gain: We use the "multipath power gain" of [18]. We note that the total signal voltage on an antenna for a narrowband signal is a phasor sum of the individual multipath voltages at the frequency of the signal, as implied by the frequency-domain transform of (1) at any single frequency f. The total power gain would be the squared magnitude of that total signal voltage gain. However, the power changes dramatically as a function of f due to frequency selectivity. Thus, it is more informative to compare the total received power averaged over frequency, which is equal to the sum of the powers of the multipath components, as defined in Eq. 9 of [18].

Note that the maximum-amplitude measured CIR peak and RT path are scaled to match. Therefore, comparing RT and measured multipath power gain is a comparison of whether the other, non-maximum-amplitude, multipath have similar powers in sum.

b) Mean Delay and RMS Delay Spread: We analyze the mean delay and RMS delay spread of each to observe differences in channel time dispersion due to multipath. These quantify signal spread and are common metrics used to estimate the inter-symbol interference duration [19]. We represent the mean delay $\bar{\tau}$ and the RMS delay spread, σ_τ, as defined in Eq. 10 and Eq. 11 of [18].

III. Results

Full results and source code for analyses are publicly available at [20]. In this section, we provide summary results to provide a comprehensive understanding of how the Sionna RT digital twin compares to measured CIRs.

A. CIR Peak Matching

The results of the peak algorithm show significant variation in the ability of Sionna RT to predict the amplitude and delays of the multipath in the measured CIR. Several examples are plotted in Fig. 3.

The best peak matching results are shown for the EBC $\rightarrow$ Guesthouse link shown in Fig. 3a and the USTAR $\rightarrow$ Guesthouse link shown in Fig. 3c. In both of these links, we can see several RT multipath (•) that align in both time and amplitude with local measured peaks. Of the 11 measured local peaks around the highest amplitude path that have power above the noise floor in the EBC $\rightarrow$ Guesthouse link, 9 align in time, and 3 align fully by matching in both time and amplitude to a predicted RT multipath. Of the 10 measured multipath peaks in the USTAR $\rightarrow$ Guesthouse link, 9 align in time, and 3 align fully with predicted RT multipath.

In contrast, in the EBC $\rightarrow$ USTAR link in Fig. 3b, the RT CIR is very different from the measured CIR. There are many measured multipath, including an initial path that arrives almost 1 μs before the maximum power path. This maximum power path is shifted in time and scaled in amplitude to align with the RT CIR as best as possible, as described in II-E.

From these statistics, our study concludes a total peak-matching percentage of 10.2% across all links in the network, where a total of 18 predicted RT multipath match in both time and amplitude to a corresponding measured CIR peak. The highest matching percentage for a single link is 27.3% in the EBC $\rightarrow$ Guesthouse link and the lowest is 0%, occurring in several of the network links.

B. Peak Matching vs. Time Delay

At what time delays is RT most accurate? To answer this question, we classify multipath in three time bins: *pre-peak* paths arrive more than 100 ns before the maximum power peak; *post-peak* paths arrive more than 100 ns after the maximum power peak; and *surrounding-peak* paths arrive within 100 ns of the maximum power peak.

Looking at the results over all links, we observe that most of the measured peaks that match with RT predicted multipath are within the surrounding-peak window, arriving within 100 ns of the most prominent peak. As shown in Table I, 13/18 or 72% of measured surrounding-peak paths are matched to RT predictions. But only 3% of paths that are not surrounding-peak paths are matched to RT predictions.

Peak Type	Matching RT Multipath	Total Measured Peaks
Pre-Peak	2	76
Surrounding-Peak	13	18
Post-Peak	3	83
Total	18	177

TABLE I: Total Measured Multipath Peaks vs. Matching RT Multipath for Entire Network, Grouped by Time of Arrival.

Only two links, EBC $\rightarrow$ USTAR and USTAR $\rightarrow$ Guesthouse, have matching pre-peak multipath, and two links, EBC $\rightarrow$ Guesthouse and USTAR $\rightarrow$ Guesthouse, have matching post-peak multipath.

C. Multipath Power Gain

Our dataset represents a wide range of multipath power gain. The smallest multipath power gain is in the USTAR $\rightarrow$ Mario link, where the measured CIR produces a multipath power gain of 0.087×10^{-12} (which corresponds to -130.6 dB) and the RT CIR produces a multipath power gain of 0.049×10^{-12} (-133.1 dB). The largest received power is in the Guesthouse $\rightarrow$ EBC link, where the measured CIR has a received power of 578×10^{-9} (-62.4 dB) and the RT CIR data has a received power of 614×10^{-9} (-62.1 dB). Note that because of the amplitude alignment of the RT and measured maximum power paths, differences mean that the other multipath do not match in amplitude. We quantify the ability of the RT to predict the gains of non-maximum power paths in Fig. 4a. The correlation coefficient is $r = 0.852$, showing a strong correlation in the multipath power gain from RT and measured CIR.

D. RMS Delay Spread and Mean Delay

To further summarize the differences between RT and the measured multipath channel, we compare their RMS delay spreads and mean delays.

The RMS delay spreads for the measured CIRs are between 0.1 and 0.5 μs, which is in the range of what is measured in other urban radio channels [21]. Fig. 4b shows the ray tracing vs. measured RMS delay spread for each of the links in the network. We observe that the RT RMS delay spreads are much lower, in the 0.0 to 0.35 μs range. On average, the measured RMS delay spread is about 3 times higher than the RT result. Table II shows the difference between measured and RT RMS delay spreads by mean, minimum, and maximum.

Further, as shown in Fig. 4b, the RT and measured RMS delay spreads are not visibly correlated – the RT and measured RMS delay spreads have a correlation coefficient of $r = -0.350$, which is quite low. This shows that the RT CIR provides a poor prediction of the time dispersion of the multipath radio channel across our dataset.

The mean transmission delay per link is also shown in Fig. 4c. In contrast to the RMS delay spreads, there is a strong linear correlation between the measured and RT mean delays with a correlation coefficient of $r = 0.997$. However,

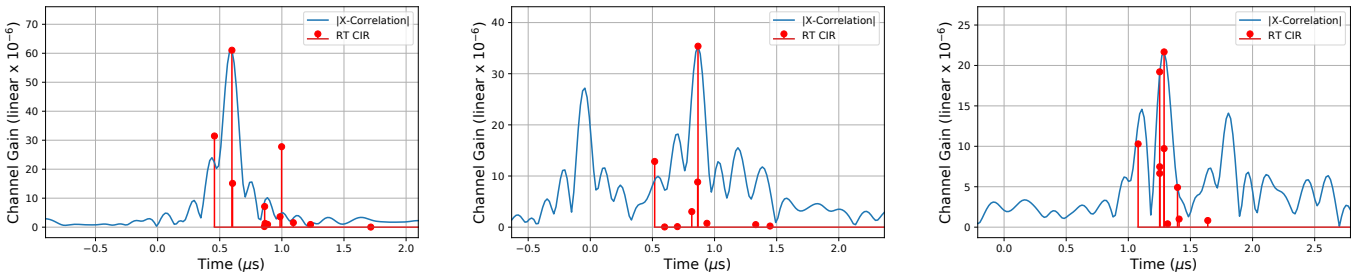

(a) EBC → Guesthouse (b) EBC → USTAR (c) USTAR → Guesthouse

Fig. 3: Comparison of measured (—) and RT (●) CIR plotted as linear channel gain vs. delay.

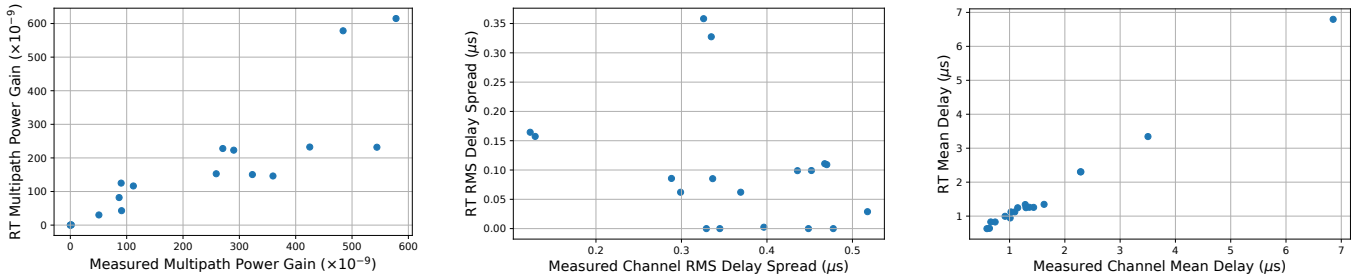

(a) Multipath Power Gains (b) RMS Delay Spreads (c) Mean Delays

Fig. 4: Scatter plots comparing statistics of the RT CIR vs. measured CIR for all links.

	Mean	Min	Max
Measured RMS Delay Spread	$0.364\mu s$	$0.123\mu s$	$0.518\mu s$
RT RMS Delay Spread	$0.097\mu s$	$0.0\mu s$	$0.358\mu s$

TABLE II: Mean, Minimum, and Maximum RMS Delay Spread for Measured Links and Ray Tracing Simulations.

we expect this correlation because the maximum power path of the measured and RT CIR are time-aligned as part of the matching procedure. The mean delays must match closely as a result.

E. Discussion

There are several reasons why late-arriving multipath are inaccurately predicted by RT. By definition, late-arriving multipath have traveled longer distances, and any inaccuracies in the scene have a higher chance of affecting them.

One source of scene inaccuracy is from the building map. Because the Sionna rendered scenes are drawn using OpenStreetMap [8], a freely editable world map [22], there are inconsistencies. Some building coordinates seem to be misaligned, on the order of meters. Building shape is simplified, e.g., as having completely flat rooftops even though there are objects and structures that protrude from the surface of the roof. Further, updates to the map are delayed. The OpenStreetMap database is built from the contributions of volunteers [22]. Thus, update delay is generally not guaranteed to be low. An example of this can be seen at the University of Utah, where a building under construction was not present in the OpenStreetMap database at the time this work was conducted, and therefore was not present in the rendered Sionna scene used for this work, as shown in Fig. 5.

Further, many static and moving objects, including trees, other vegetation, vehicles, and people are not in the rendered scene. In particular there are many trees along the roadways. The dense deployment nodes are also along roadways at 8.8 m or 11.3 m above the ground [17], and due to the varying terrain, objects on the ground can obstruct (or create) paths between nodes.

The real-world factors discussed above impact radio channels in ways that are currently extremely difficult to dynamically model in RT. These factors should be considered when designing enhancements to digital twins to more accurately simulate signal behavior in a real-world environment.

On the measurement side, improved measurements could help distinguish multipath. Bandwidth is a major limitation: the C-band has limited interference-free bandwidth near the testbed, and further, the maximum sampling rate of the NI/Ettus B210 radios in dense deployment nodes is 56 MHz. Chips are SRRC pulse-shaped and thus have sidelobes, which can appear to be multipath peaks. In future work, it may be beneficial to use a superresolution method to estimate multipath delays and amplitudes at a higher resolution [23]. Using a mobile transmitter or receiver would also increase the number of spatially distinct measurements in the dataset, allowing more comparison results to be presented.

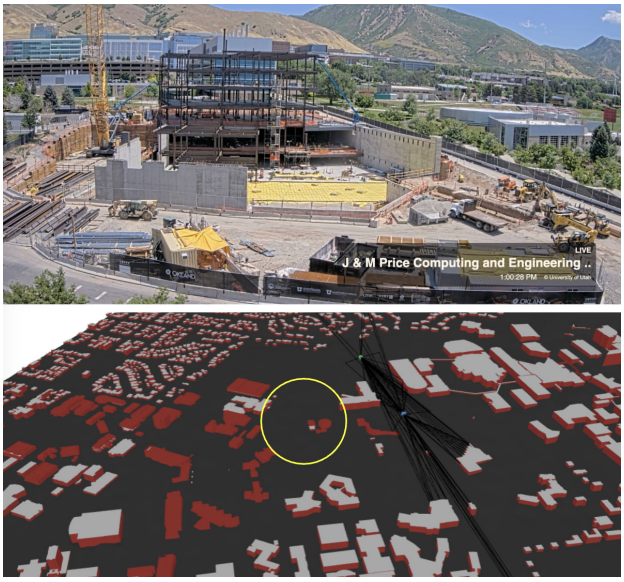

Fig. 5: Image from construction webcam (top) of new building absent in the rendered Sionna scene (bottom).

IV. Conclusion

We present a comparative analysis between a Sionna ray tracing-based digital twin and measured CIR measurements in a large-scale outdoor testbed. We introduce methods to compare time delays and amplitudes of multipath components. The results in this study show the limitations of relying on RT to fully model observed multipath radio channels for future digital RF twins. For example, 10.2% of measured multipath components are similar in amplitude and time delay to RT-predicted paths. The methods used in this study can be generalized to other RT software and measurements on other wireless testbeds for further comparative analysis. Future work is needed to improve RT to better match measured CIR and for channel measurements that allow validation of other multipath data predicted by RT, such as angle-of-arrival.

Acknowledgment

The authors thank Serhat Tadik for setting up the Sionna RT software.

References

[1] S. Mihai, M. Yaqoob, D. V. Hung, W. Davis, P. Towakel, M. Raza, M. Karamanoglu, B. Barn, D. Shetve, R. V. Prasad, H. Venkataraman, R. Trestian, and H. X. Nguyen, "Digital twins: A survey on enabling technologies, challenges, trends and future prospects," *IEEE Communications Surveys & Tutorials*, vol. 24, no. 4, pp. 2255–2291, 2022.

[2] Y. Thomas, S. Toumpis, and N. Smyrnioudis, "Digital twin approach to estimating and utilizing the capacity region of wireless ad hoc networks," *Computer Networks*, vol. 241, no. C, Mar. 2024.

[3] S. Zelenbaba, "Digital twin for reliable wireless communications," Ph.D. dissertation, Technische Universität Wien, 2022.

[4] G. D. Durgin, M. A. Varner, N. Patwari, S. K. Kasera, and J. Van der Merwe, "Digital spectrum twinning for next-generation spectrum management and metering," in *2022 IEEE 2nd Intl. Conf. on Digital Twins and Parallel Intelligence (DTPI)*, 2022, pp. 1–6.

[5] R. Kumahia, U. Demir, S. Pradhan, B. Salehihikouei, K. Chowdhury, and S. Ioannidis, "DITTO: Digital twins for testing and optimizing wireless decisions," in *2024 IEEE Intl. Conf. on Metaverse Computing, Networking, and Applications (MetaCom)*, 2024, pp. 121–128.

[6] Z. Yun and M. F. Iskander, "Ray tracing for radio propagation modeling: Principles and applications," *IEEE Access*, vol. 3, pp. 1089–1100, 2015.

[7] J. Breen, A. Buffmire, J. Duerig, K. Dutt, E. Eide, G. Anneswa, M. Hibler, D. Johnson, S. K. Kasera, E. Lewis, D. Maas, C. Martin, A. Orange, N. Patwari, D. Reading, R. Ricci, D. Schurig, L. B. Stoller, A. Todd, J. V. d. Merwe, N. Viswanathan, K. Webb, and G. Wong, "Powder: Platform for open wireless data-driven experimental research," *Computer Networks*, vol. 197, 2021.

[8] J. Hoydis, F. Aoudia, S. Cammerer, M. Nimier-David, N. Binder, G. Marcus, and A. Keller, "Sionna RT: Differentiable ray tracing for radio propagation modeling," in *2023 IEEE Globecom Workshops*, Dec. 2023, pp. 317–321.

[9] J. Nuckelt, T. Abbas, F. Tufvesson, C. Mecklenbrauker, L. Bernado, and T. Kurner, "Comparison of ray tracing and channel-sounder measurements for vehicular communications," in *2013 IEEE 77th Vehicular Technology Conference (VTC Spring)*, 2013, pp. 1–5.

[10] P. Paschalidis, J. Nuckelt, K. Mahler, M. Peter, A. Kortke, M. Wisotzki, W. Keusgen, and T. Kürner, "Investigation of MPC correlation and angular characteristics in the vehicular urban intersection channel using channel sounding and ray tracing," *IEEE Transactions on Vehicular Technology*, vol. 65, no. 8, pp. 5874–5886, 2015.

[11] H. Hashemi, "Simulation of the urban radio propagation channel," *IEEE Transactions on Vehicular Technology*, vol. 28, no. 3, pp. 213–225, 1979.

[12] R. Mutagi, "Pseudo noise sequences for engineers," *Electronics & Communication Engineering Journal*, vol. 8, no. 2, pp. 79–87, 04 1996.

[13] G. Jacovitti and G. Scarano, "Discrete time techniques for time delay estimation," *IEEE Transactions on Signal Processing*, vol. 41, no. 2, pp. 525–533, 1993.

[14] C. Jeng and N. Patwari, "WATCH: A distributed clock time offset estimation tool for software-defined radio platforms," in *IEEE INFOCOM 2024 - IEEE Conference on Computer Communications Workshops*, Vancouver, BC, Canada, 2024, pp. 1–6.

[15] C. Jeng, N. Patwari, A. Singh, J. Wang, and M. G. Weldegebriel, "OTA CIR measurements on POWDER," 01 2025, https://colab.research.google.com/drive/1qUp7MgBtZ0hp3xUQEjaLpNL7Er2nQ7RM.

[16] K. Webb, S. K. Kasera, N. Patwari, and J. Van der Merwe, "WiMatch: Wireless resource matchmaking," in *IEEE INFOCOM 2021-IEEE Conference on Computer Communications Workshops*, 2021, pp. 1–6.

[17] Flux Lab Gitlab, "POWDER Node Locations," 2025, https://gitlab.flux.utah.edu/powderrenewpublic/powder-deployment/-/blob/master/powder-deployment.csv.

[18] A. A. Saleh and R. Valenzuela, "A statistical model for indoor multipath propagation," *IEEE Journal on Selected Areas in Communications*, vol. 5, no. 2, pp. 128–137, 1987.

[19] M. Varela and M. Sánchez, "RMS delay and coherence bandwidth measurements in indoor radio channels in the UHF band," *IEEE Transactions on Vehicular Technology*, vol. 50, no. 2, pp. 515–525, 03 2001.

[20] C. Jeng, "CIR comparison," April 2025, https://github.com/cjeng8771/CIRcomparison.

[21] I. T. Union, "Propagation data and prediction methods for the planning of short-range outdoor radiocommunication systems and radio local area networks in the frequency range 300 MHz to 100 GHz," in *Recommendation ITU-R P.1411-13*, 09 2025.

[22] A. Grinberger, M. Minghini, L. Juhász, G. Yeboah, and P. Mooney, "OSM science - the academic study of the OpenStreetMap project, data, contributors, community, and applications," *ISPRS International Journal of Geo-Information*, vol. 11, no. 230, 2022.

[23] R. Vaughan and N. Scott, "Super-resolution of pulsed multipath channels for delay spread characterization," *IEEE Transactions on Communications*, vol. 47, no. 3, pp. 343–347, 1999.